JGR Oceans

RESEARCH ARTICLE
10.1029/2025JC022921

Sensitivity of Dynamical Downscaling in the Northern Adriatic Sea

Renata Tatsch Eidt[1,2], Giorgia Verri[2], Vladimir Santos da Costa[2], Anna Katavouta[3], and Antonio Navarra[2,4]

[1]Department of Physics and Astronomy, University of Bologna, Bologna, Italy, [2]CMCC Foundation—Euro-Mediterranean Center on Climate Change, Lecce, Italy, [3]Marine Systems Modelling, National Oceanography Centre, Liverpool, UK, [4]Department of Biological, Geological, and Environmental Sciences, University of Bologna, Bologna, Italy

Abstract This study evaluates the performance of dynamical downscaling in the Northern Adriatic Sea, focusing on eddy kinetic energy spectra and dense water formation. Using the perfect model framework, a high-resolution (2 km) reference simulation of the entire Adriatic Sea serves as the benchmark for a series of one-way nesting downscaling experiments reaching the same horizontal resolution in the Northern Adriatic. Results show that a downscaling ratio of 1:3 effectively reproduces the local energy budget and multiscale features. However, the absence of feedback from small to large scales limits the downscaling performance. This limitation is evident in dense water formation, which is controlled by the interplay between local and remote drivers in the Northern Adriatic Sea. When local drivers, such as buoyancy fluxes, dominate, the dense water formation process is well reproduced. In contrast, when remote influences, particularly the inflow of salty Levantine Intermediate Water through the Otranto Strait, are not properly resolved by the parent model, reproducibility of dense water formation deteriorates. Our experiments indicate that a 2 km horizontal resolution effectively captures cross-scale interactions at the strait, while a 6 km resolution is insufficient. These interactions, particularly feedback from small scales to large scales, lead to changes in thermohaline dynamics that propagate toward the Northern Adriatic Sea.

Plain Language Summary Downscaling is a common technique used in ocean prediction models to take large-scale information and refine it for local applications. To ensure the reliability of these predictions, it is important to understand the strengths and limitations of the downscaling method. In this study, we applied the "perfect model approach" to evaluate the performance of our downscaling technique in the Northern Adriatic Sea, focusing on the accuracy of local physical processes and multiscale features. Our results indicate that a 1:3 resolution ratio up to 2 km is effective for refining predictions in this region. We also found that both local and remote factors significantly influence the formation of dense water in the Northern Adriatic. When remote drivers, such as the inflow of saltier water through the Otranto Strait, are poorly represented by the parent model, the accuracy of local predictions decreases. However, when local drivers prevail, such as the wintertime heat loss, the downscaling method performs well even if the ocean conditions are not well represented in the parent model. These findings offer insights for improving forecasting systems in marginal seas and may have broader relevance for similar coastal regions worldwide.

Key Points:

- Effective downscaling requires both representation of local small-scale processes and consistent large-scale boundary conditions
- Cross-scale interactions preserved in parent fields improve EKE recovery and dense water reproducibility in one-way nesting strategies
- Otranto Strait dynamics modulate remote effects on thermohaline properties and dense water formation in the Northern Adriatic

Supporting Information:

Supporting Information may be found in the online version of this article.

Correspondence to:

R. T. Eidt,
renata.eidt@cmcc.it

Citation:

Eidt, R. T., Verri, G., Santos da Costa, V., Katavouta, A., & Navarra, A. (2026). Sensitivity of dynamical downscaling in the Northern Adriatic Sea. *Journal of Geophysical Research: Oceans*, *131*, e2025JC022921. https://doi.org/10.1029/2025JC022921

Received 23 MAY 2025
Accepted 21 DEC 2025

Author Contributions:

Conceptualization: Renata Tatsch Eidt, Giorgia Verri, Antonio Navarra
Data curation: Renata Tatsch Eidt
Formal analysis: Renata Tatsch Eidt, Giorgia Verri, Vladimir Santos da Costa, Anna Katavouta
Funding acquisition: Giorgia Verri
Investigation: Renata Tatsch Eidt
Methodology: Renata Tatsch Eidt, Giorgia Verri, Vladimir Santos da Costa, Anna Katavouta
Project administration: Giorgia Verri, Antonio Navarra
Resources: Giorgia Verri, Anna Katavouta, Antonio Navarra

1. Introduction

The Adriatic Sea is shaped by the interplay between local and remote processes, which modulate its circulation and water mass transformations. Its semienclosed configuration, complex orography, and strong air-sea interactions make it a natural laboratory for numerical ocean modeling (Umgiesser et al., 2022), providing an ideal setting for testing modeling approaches and investigating multiscale dynamics in marginal seas. Regional to coastal downscaling has become a crucial approach for this purpose, allowing coarse-resolution patterns to be refined and providing high-resolution information at local scales, thereby enabling a detailed representation of multiscale coastal processes while maintaining reasonable computational costs.

Increasing model resolution generally enhances the representation of oceanic features that are not resolved by coarser models (Chassignet et al., 2020; Fox-Kemper et al., 2019). Downscaling strategies are therefore expected to reproduce the small-scale variability and effectively capture cross-scale interactions. Accurately reproducing the mesoscale circulation is essential when studying ocean dynamics due to its role in momentum, salt, and heat transport and in modulating the ocean energy budget. In the Mediterranean Sea, mesoscale features have a strong

Software: Renata Tatsch Eidt, Giorgia Verri, Vladimir Santos da Costa, Anna Katavouta
Supervision: Giorgia Verri, Vladimir Santos da Costa, Anna Katavouta, Antonio Navarra
Validation: Renata Tatsch Eidt
Visualization: Renata Tatsch Eidt
Writing – original draft: Renata Tatsch Eidt
Writing – review & editing: Renata Tatsch Eidt, Giorgia Verri, Vladimir Santos da Costa, Anna Katavouta, Antonio Navarra

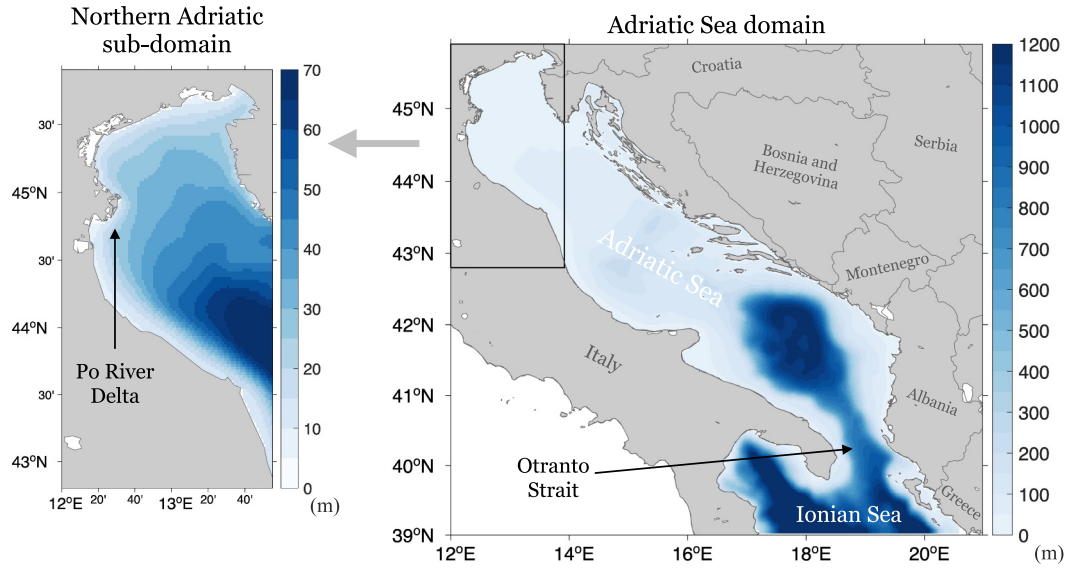

Figure 1. Bathymetry (m) of the Adriatic Sea domain (right) and the nested Northern Adriatic subdomain with a refined color scale (left). Important features, including the Otranto Strait (connecting the Adriatic to the Ionian Sea and Mediterranean) and the Po River Delta in the Northern Adriatic, are indicated with arrows.

contribution to sea-surface height variability and kinetic energy (Bonaduce et al., 2021) and can have a significant impact in the formation and spreading of water masses (Gascard, 1978).

Mesoscale eddies contain most of the ocean's kinetic energy (Ferrari & Wunsch, 2009) with their characteristic length scales varying depending on the region (Hallberg, 2013). Properly resolving these mesoscale features requires eddy-resolving models with small enough grid spacing to capture the baroclinic instabilities associated with these eddies (Hallberg, 2013; Hurlburt et al., 2008). In coastal regions, these resolution requirements become even more challenging due to the reduced Rossby radius and increased topographic complexity (Pinardi et al., 2006). In the Middle Adriatic Sea, mesoscale eddies typically range from 10 to 20 km, expanding as they move toward the open sea (Paschini et al., 1993). Additionally, seasonal variability influences the vertical structure of the water column in shallow seas, modulating the spatial scales of baroclinic instabilities and, consequently, the resolution requirements for resolving them. This is particularly evident in strongly stratified regions, such as the meanders along the Italian coast of the Adriatic Sea (Cushman-Roisin et al., 2007).

The Adriatic Sea connects southward to the Ionian Sea (Figure 1) and has significant contribution to the large thermohaline circulation of the Mediterranean Sea (Pinardi et al., 2006). This connection occurs through the narrow Otranto Strait where substantial salt and heat exchanges modulate the basin's properties (Astraldi et al., 1999; Vilibić & Orlić, 2002; Yari et al., 2012). Due to its landlocked morphology, the Adriatic is highly influenced by variable atmospheric conditions and winds that affect the near-surface circulation and heat fluxes and contribute to dense water formation (Artegiani et al., 1997b; Cushman-Roisin et al., 2013; Vilibić & Supić, 2005).

The Northern Adriatic Sea is particularly susceptible to local atmospheric forcing and river discharges especially from the Po River (Cushman-Roisin et al., 2013). The shallow nature of this sub-basin makes it extremely sensitive to seasonal variability, transitioning from mixed to stratified conditions. It is a key region for dense water formation, particularly the North Adriatic Dense Water (NAdDW), which is produced during winter especially under strong Bora wind events (Artegiani et al., 1997a; Vilibić & Supić, 2005; Zore-Armanda, 1963). The significance of this dense water formation site makes the Northern Adriatic Sea a crucial contributor to the general Mediterranean thermohaline circulation and strongly influences the deep water properties of the basin (Pinardi et al., 2006).

Together with the predominant influence of local factors such as heat fluxes and river discharge, thermohaline variability in the Northern Adriatic is also affected by remote forcing. With a main basin-wide cyclonic

(counterclockwise) circulation pattern (Artegiani et al., 1997a; Cushman-Roisin et al., 2013), water properties in the northern sub-basin are also modulated by the advection of southern waters toward the north. The potential impact of large-scale oscillatory modes, such as the Adriatic-Ionian Bimodal Oscillating System (BiOS), on the Northern Adriatic remained unclear until recently. Vilibić et al. (2020) provided evidence that the BiOS regime in the northern Ionian Sea is correlated with salinity variability in the Northern Adriatic. The BiOS has been defined as a feedback mechanism (Gačić et al., 2010) linking the Ionian circulation patterns to dense water formation in the Adriatic Sea. The near surface circulation regime of the Northern Ionian Gyre (NIG), whether cyclonic or anticyclonic, preconditions the entrance of either eastern or western Mediterranean waters, respectively, toward the Adriatic (Gačić et al., 2010; Liu et al., 2022; Pinardi et al., 2015). In the northern sub-basin, however, the dominance of local forcing leads to a lack of detectable remote signals such as the BiOS at interannual to decadal scales (Denamiel et al., 2022).

Modeling marginal seas such as the Adriatic can be challenging due to their complex geomorphology and river inputs. Being a dilution basin, an accurate representation of the wind and buoyancy forcings is essential for modeling the Adriatic circulation and water mass transformations. In particular, high-resolution wind fields are required to capture Bora outbreaks, which strongly affect dense water formation. Coarse-resolution reanalyses, such as ERA5, have been shown to underestimate Bora intensity, introducing biases in simulating both severe events and the long-term thermohaline circulation of the Adriatic-Ionian system (Denamiel et al., 2021). Regarding river inputs, outdated climatologies may introduce significant biases in the salinity field (Pranić et al., 2023) also affecting dense water formation. River runoff has been shown to influence both local thermohaline variability and basin-scale processes, such as the Adriatic meridional overturning circulation (Verri et al., 2018). The Po River, in particular, accounts for nearly 30% of the Adriatic Sea's annual discharge and is the largest freshwater source for the Central Mediterranean (Cushman-Roisin et al., 2013), making its accurate representation essential for simulating this basin dynamics (Verri et al., 2020).

Several studies have used the Adriatic as a benchmark for testing numerical approaches in marginal seas (Umgiesser et al., 2022). Early modeling efforts highlighted the sensitivity of dense water formation to atmospheric forcing, including heat fluxes and wind stress (Vested et al., 1998), and more specifically to Bora driven events (Paklar et al., 2001). Recent studies have emphasized the importance of coupled atmosphere-ocean representation for capturing extreme Bora episodes (Ličer et al., 2016). Kilometer-scale systems, combining high-resolution atmospheric models with ocean models approaching 1 km resolution, have demonstrated the added value of such coupling for capturing dense water dynamics (Denamiel et al., 2019, 2021; Pranić et al., 2024) over multidecadal timescales (Pranić et al., 2021, 2023). Nested regional modeling has also been used to investigate local processes and applications, such as marine renewable energy (Giordano et al., 2024) and the assessment of coastal hazards and flooding (Torresan et al., 2019; Umgiesser et al., 2021). Finally, climate projections with regional modeling systems have recently been applied to explore the future evolution of the Adriatic under climate change scenarios (Verri et al., 2024; da Costa et al., 2024).

This study aims to evaluate how effective are downscaling strategies in capturing the local small-scale features of the Northern Adriatic Sea dynamics as well as key wider physical processes in the basin, such as dense water formation. These objectives are addressed with the use of the "perfect model" approach (Boer, 2004; De Elia et al., 2002). The name "perfect model" does not imply that the target model is anywhere perfect but rather indicates a numerical experiment design that considers one model simulation as the reference point for sensitivity and other studies.

Also referred to as "big-brother" experiment, the use of the perfect model framework for downscaling studies typically involves using a high-resolution, large domain reference simulation as the "truth", and nesting smaller downscaling experiments into a coarser resolution parent model. Downscaling performance is finally evaluated by comparing the child experiments to the reference "truth" solution. The method suggests that, instead of relying on observational data, model simulations can serve as a reference, or "truth", for evaluating what can be called "perfect model predictability" (Liu et al., 2019). This approach eliminates the uncertainties associated with observational errors and model inaccuracies (Denis et al., 2002).

The perfect model approach has been applied across a range of contexts in climate science, including internal variability assessment, predictability studies (Ortega et al., 2017; Persechino et al., 2013; Liu et al., 2019) and model drift analysis (Boer, 2004). Within regional modeling, it has been widely used for evaluation of

atmospheric downscaling strategies (De Elia et al., 2002; Denis et al., 2002; Skamarock et al., 2018), although applications for ocean purposes still remain limited (Pham et al., 2016; Pham & Hwang, 2020).

In this study, the "truth" is represented by a high-resolution (2 km) simulation of the entire Adriatic Sea used as a reference for nested downscaling experiments in the Northern Adriatic. The aim is to evaluate how well the child experiments reproduce the local energy field (kinetic energy) and key physical processes (dense water formation). By addressing challenges such as the reproducibility of mesoscale patterns and the influence of complex marginal-sea geometry on cross-scale processes, this work seeks to advance coastal ocean modeling via dynamical downscaling and provide new insights into the thermohaline dynamics of the Northern Adriatic.

The paper is organized as follows: Section 2 describes the methodology, including the ocean model configuration and forcing fields, the perfect model framework, and the experimental setup. Sections 3 and 4 present and discuss the results, focusing on the reproducibility of energy spectra across different downscaling strategies (Section 3) and the reproducibility of physical processes, particularly dense water formation in the Northern Adriatic (Section 4). Section 5 summarizes the findings, including the strengths and limitations of the downscaling approaches, insights into the drivers of dense water variability, and implications for future coastal ocean modeling studies.

2. Methodology

2.1. The Ocean Model Configuration and Driving Fields

The ocean model used for this downscaling study is the finite difference Nucleus for European Modeling of the Ocean (NEMO v3.6) (Madec et al., 2017), which solves the primitive equations in an Arakawa C-type structured grid. The model configuration incorporates the Adriatic Sea bathymetry from the European Marine Observation and Data Network (EMODnet, 2020), featuring a high horizontal resolution of 3.75 arc s to accurately represent the region's complex morphology and coastlines.

Horizontal subgrid-scale mixing for both tracers and momentum was represented using a bilaplacian operator with constant viscosity and diffusivity coefficients. Momentum advection was performed in vector/flux form using a centered scheme, whereas tracer advection employed the MUSCL (Monotone Upstream Scheme for Conservative Laws) scheme. Vertical mixing of tracers and momentum was parameterized with the TKE turbulent closure scheme (Gaspar et al., 1990). Vertical advection for both tracers and momentum was computed using an implicit Euler backward scheme. No-slip boundary conditions and nonlinear bottom friction were applied at lateral land and bottom boundaries, respectively.

Initial conditions were obtained from the Copernicus Marine Environment Monitoring Service (CMEMS) reanalysis product for the Mediterranean Sea (Escudier et al., 2021). Daily averaged temperature and salinity fields with a horizontal resolution of $1/24°$ and 141 unevenly distributed z* levels were bi-linearly interpolated to the model grid. For the scope of the downscaling study, directed to a climate perspective on a multiannual basis, tides were not included in the simulations.

The large-domain experiments, covering the entire Adriatic Sea, feature a southern open boundary at latitude 39°N, connecting to the Ionian Sea. Lateral boundary conditions, including temperature, salinity, baroclinic and barotropic velocities, and sea surface height, were derived from the same CMEMS reanalysis product. Barotropic velocities at the open boundary in this case were implemented using the Flather scheme (Flather, 1976). Tracer fields and baroclinic velocities were imposed directly from the boundary fields (i.e., CMEMS reanalysis). To preserve total volume transport at the boundary, an "interpolation constraint" (Pinardi et al., 2003) was applied. This ensured that, after interpolation, the normal velocity field at the nested boundary matched the original parent model's volume transport.

For the implementation of the lateral open boundary of the child experiments in the Northern Adriatic subdomain, again the Flather radiation scheme (Flather, 1976) was adopted for the barotropic velocities. For tracers and baroclinic velocities, the Orlanski scheme with radiation plus relaxation algorithm was used (Marchesiello et al., 2001) with a sponge layer of 5 grid points and an inflow and outflow damping timescale of 1 and 30 days, respectively.

The atmospheric fields forced at the surface boundary are derived from the Integrated Forecasting System (IFS) analysis product of the European Center for Medium-Range Weather Forecasts (ECMWF) with a horizontal

resolution of 0.125° and a frequency of 6 hr. Precipitation data were obtained from the ECMWF reanalysis product ERA5 (Hersbach et al., 2020) with a resolution of 0.25° and a frequency of 1 hr. These atmospheric fields were interpolated to the model grid using bi-linear interpolation for most fields and bi-cubic interpolation for wind components. Air-sea fluxes were then computed using the Mediterranean Forecasting System (MFS) bulk formulae (Castellari et al., 1998).

The choice of the IFS analysis product over a reanalysis product was motivated by its relatively high horizontal resolution, which provides improved representation of local surface atmospheric conditions, including wind outbreaks that play a crucial role in dense water formation. Nevertheless, this resolution remains insufficient to fully resolve Bora wind dynamics, which may require dedicated atmospheric models at 3 km or finer (Denamiel et al., 2021). As a result, the model may underestimate the intensity and spatial distribution of Bora events potentially affecting dense water generation. However, for the intended purpose of climate-oriented, multiannual downscaling experiments, the adopted atmospheric forcing can be considered appropriate, even if individual Bora events are less accurately represented.

River inputs are prescribed at their respective river mouths in terms of volume flux and salinity, implemented as surface sources at the border grid cell within the model domain. Salinity is set to a constant value of 17 PSU for the Po River and 15 PSU for all other rivers based on previous studies (Verri et al., 2018) and sensitivity tests (Oddo et al., 2005; Simoncelli et al., 2011) for the region. In total, 63 river catchments are included in the model domain. All rivers are implemented as point sources except for two coastal regions where runoff is distributed across multiple grid points (i.e., Marche and Abruzzo and Molise regions), representing diffused sources.

Runoff data for most rivers are based on monthly climatologies, converted into daily values using linear interpolation, following (Killworth, 1996) for conserving the correct monthly means. These climatologies originate primarily from the data set described by Verri et al. (2018) with the exception of the Adige, Isonzo, Reno, Tronto, Brenta, and Piave rivers for which more recent data sets were used (CNR-ISMAR). A recent revise of the freshwater discharge into the Adriatic Sea by Aragão et al. (2024) confirms the good quality of the runoff climatologies adopted within this study. The Po River discharge is instead based on daily mean runoff data from the Pontelagoscuro station (approximately 40 km upstream of the delta) provided by Arpae Emilia-Romagna (https://simc.arpae.it). For this specific case, using daily observations rather than monthly climatologies may better resolve the high frequency variability of freshwater input, since the Po River has major impact on Adriatic dynamics. The total runoff from this catchment is divided into nine river mouths within the model domain corresponding to the branches of the Po River delta, which are unequally distributed following the proportions reported by Provini et al. (1992).

2.2. The Perfect Model Approach Over the Adriatic Sea

With the aim of evaluating the effectiveness of dynamical downscaling over the Northern Adriatic Sea, the perfect model framework is considered. In this context, the perfect model approach (De Elia et al., 2002) is implemented as a set of dynamical nesting sensitivity experiments. This methodology, which relies on an idealized high-resolution simulation serving as the reference for downscaling assessments, is also referred to as the "big brother" experiment (Denis et al., 2002, 2003; Pham & Hwang, 2020).

The "truth" experiment, referred to as L2, covers the entire Adriatic Sea at a horizontal resolution of $1/48°$ and is considered the benchmark for assessing the performance of downscaling experiments. The downscaling experiments are conducted over a smaller domain in the Northern Adriatic Sea, preserving the same high resolution of the "truth" ($1/48°$) while being nested within parent experiments of varying, coarser resolutions. The parent experiments, such as the L2 experiment, cover the entire Adriatic but differ in horizontal resolution. For evaluation of downscaling performance, the results of the child experiments are compared to the corresponding region within the "truth" reference experiment. Figure 2 provides a schematic overview of the perfect model approach over the Adriatic Sea.

In a usual perfect model setup, the coarse parent driving fields are obtained statistically by applying a low-pass filter to the reference "truth" solution, imitating a low resolution parent model (De Elia et al., 2002). Here, a novel approach to this method is introduced, integrating both filtered and dynamically generated parent fields for driving the refined resolution nested experiments.

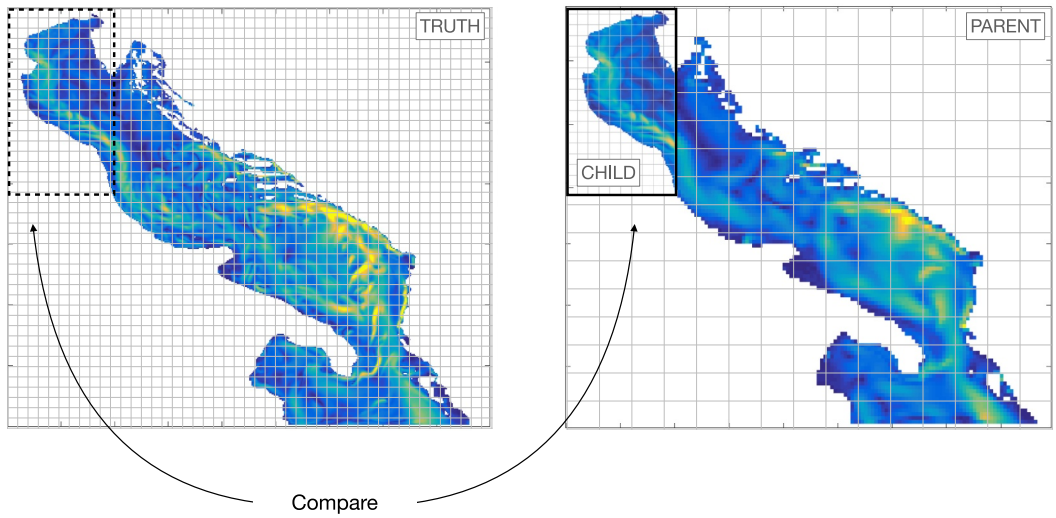

Figure 2. Schematic representation of the perfect model approach for the Adriatic Sea with the northern subregion as a nested child domain. On the left is the large-domain high-resolution experiment ("truth"), and on the right is the downscaling experimental setting. The child experiment (right) is finally compared with the corresponding area of the "truth" experiment (left). Shading represents daily surface velocity outputs for illustration.

The value of the perfect-model approach is complementary to the one of performing a traditional model validation by comparison with observations. It allows to identify the effects specifically related to the implementation of lateral open boundaries by providing a target for modeling performance. Comparisons between the child experiments and the "truth" experiment provide means to judge the downscaling methodology and the nesting strategy. In the next sections, we examine the ability of the downscaling to reproduce small-scale features and capture multiscale and cross-scale dynamics within a one-way nesting framework.

Although the present study focuses on a perfect model framework, the reference "truth" experiment covering the Adriatic Sea at a 2 km horizontal resolution has been evaluated against available observations and reanalysis data. A brief comparison with the CMEMS Mediterranean reanalysis (see Supporting Information S1, Section 1) shows that the model captures the main features of the Adriatic circulation, including the coastal Po River plume, with small temperature and salinity differences. These differences are consistent with the higher coastal resolution of L2, the explicit representation of river discharge, the choice of atmospheric forcing, and the absence of data assimilation. Overall, this comparison indicates that the L2 model provides a suitable representation of the Adriatic system for the intended perfect-model study.

2.3. The Experimental Setting

The series of experiments span a 19 years time window from 2001 to 2019. The resolution of the child experiment in the Northern Adriatic domain is always the same as the "truth" L2, that is, $1/48°$ (~2 km), as shown in Figure 2. What changes is the horizontal resolution of the parent experiments proposed and consequently the downscaling ratio assumed in each strategy.

The downscaling experiments were implemented using a one-way nesting approach in which the child domains are forced at the lateral boundaries by the parent model without feedback to the parent grid. Although here the term "downscaling" is used to describe the transition from coarser to finer resolution, this differs from other downscaling techniques, such as spectral nudging, where large-scale dynamics are imposed throughout the interior of the domain.

The same z-geopotential vertical coordinate discretization is employed for all experiments, featuring 120 levels spanning from 1.2 to 2,600 m. A partial step configuration was adopted, which adjusts the bottom layer thickness to align with the real topography, allowing for a more accurate representation of bathymetry. The vertical grid is unevenly distributed with a stretching function with higher density of layers near the surface.

Table 1
Overview of Experiments

Parent	Resolution	Viscosity ($m^4\ s^{-1}$)	Diffusivity ($m^4\ s^{-1}$)	Child	Downscaling ratio
L2	1/48°	-5.00×10^7	-3.00×10^7	S2	1:1
L6	1/16°	-4.05×10^9	-2.43×10^9	S6	1:3
L10	1/10°	-3.10×10^{10}	-1.80×10^{10}	S10	1:5
L2F	∼1/10°	–	–	S2F	∼1:5

Note. Horizontal resolution and eddy viscosity/diffusivity coefficients are defined for the parent experiments, whereas all child experiments share the same values as the reference L2. The L2F parent is obtained by statistical filtering of L2 (not dynamically generated) and therefore has no mixing parameters.

In previous studies adopting the perfect model framework (De Elia et al., 2002; Denis et al., 2002; Pham & Hwang, 2020), low-resolution boundary conditions for downscaling experiments were typically generated by filtering the high-resolution "truth" experiment. This method uses a low-pass filter to remove small-scale features, retaining only large-scale components to simulate a coarse-resolution model. In this study, this approach was used alongside an alternative method resulting in two distinct strategies: (a) a filtered parent experiment (L2F), created by low-pass filtering the high-resolution L2 experiment, that is, using the "truth" large scales that have been shaped by small scales; (b) coarse resolution numerical experiments (L6 and L10), that is, using a model estimate of large scales that has not been shaped by the small scales.

Approach 1 allows to evaluate downscaling performance when parent large-scale features are modulated by interactions with the small-scales. On the other hand, Approach 2 follows the conventional dynamical downscaling method where high-resolution models are nested within coarser-resolution models. This allows for assessing the limitations of nesting solutions from coarse-resolution models without any explicit interaction or exchange with the small scales.

The parent and child experiments are summarized in Table 1 with nomenclature reflecting horizontal resolution in kilometers and child (small domain) experiments being named after their respective parent (large domain). L2 represents the "truth" experiment with a resolution of 1/48° (2 km), whereas L6 and L10 correspond to dynamically generated parent experiments with resolutions of 1/16° (6 km) and 1/10° (10 km), respectively. L2F represents low-pass filtered "truth" L2 parent experiment.

The filtered parent experiment L2F from Approach 1 was created by applying a low-pass Gaussian filter to the high-resolution "truth" experiment (L2). The purpose was to remove the small-scale variability and produce a solution that would mimic a coarse-resolution model, however, conserving the "truth" large scales. The filtering was applied horizontally at each vertical layer of the full L2 domain and consistently to all variables, creating a fully 3D filtered solution. To avoid inconsistencies near the coast, a "sea-over-land" step (Dominicis et al., 2014; Kara et al., 2007) was applied prior to filtering in order to extrapolate sea values across land points. The coarse experiment L10 served as a reference for selecting filter parameters primarily through comparisons of kinetic energy and currents. Sensitivity analysis determined appropriate filter settings with a window of 20 grid points and a standard deviation of 6 grid points.

All parent fields from both Approaches 1 and 2 as well as the child outputs were at daily mean frequency, and the low-pass filtering in Approach 1 was applied only in space not in time. It should be noticed that the filter suppresses fine-scale structures, but it cannot eliminate the influence of smaller-scale processes or higher-frequency events that may have shaped the large-scale fields, whose effects may still be present in the filtered solution.

Each coarse resolution parent experiment from Approach 2 was designed ensuring that the only difference among them is the horizontal resolution. Constant values of eddy viscosity and diffusivity coefficients were initially chosen based on the CMEMS reanalysis system, whose parameter settings are supported by sensitivity studies. For our 2 km reference experiment (L2), the coefficients were scaled accordingly to match the finer grid resolution. The same coefficients were applied to all child experiments, as they share the same horizontal resolution. For each parent experiment, the coefficients were further adjusted according to the respective grid spacing (see Table 1), following the relationship $a = a_0(\Delta x_S/\Delta x_L)^4$, where a_0 is the parent coefficient, Δx_S is the nested grid spacing, and Δx_L is the parent model grid spacing. Additionally, using a time-splitting technique (Shchepetkin &

McWilliams, 2005), the baroclinic and barotropic time steps for each experiment were, respectively, 120 and 2 s for L2 and all downscaling experiments, 200 and 3 s for L6, and 240 and 4 s for L10.

All child experiments maintain the same resolution as the "truth" L2, $1/48°$, with identical model configuration and time step but covering the smaller domain of the Northern Adriatic. Due to the shallower nature of this sub-basin, with a maximum depth of approximately 70 m (Figure 1), a reduced number of vertical levels remains present for the downscaling configuration. Nevertheless, 35 vertical layers are maintained, which can be considered as a highly detailed discretization for the region.

In typical downscaling implementations, resolution is increased both horizontally and vertically in the nested model configuration. However, this study focuses on a mechanistic approach where only the horizontal spacing between the parent and child domains is adjusted with the downscaled experiment reaching the same resolution as the "truth" experiment. Introducing a vertical downscaling ratio would have added another layer of complexity, as it could affect the representation of vertical dynamics and turbulent mixing, introducing additional uncertainty into the discussion.

The set of downscaling experiments is detailed in Table 1. Two experiments, S6 and S10, are driven by coarse-resolution parent simulations (L6 and L10), representing realistic one-way nesting scenarios in which the influence of smaller-scale processes in the parent model is included only through subgrid parameterizations. In contrast, S2F corresponds to downscaling from a spatially filtered version of the "truth" (L2F) following the typical perfect model framework. In this configuration, the parent fields retain only the large-scale components of the "truth", which have, however, already been shaped by cross-scale interactions in the original high resolution simulation (L2). Finally, a control experiment, which can be referred to as "best nesting", was performed using S2 nested in L2. In this case, both parent (L2) and child (S2) simulations have the same horizontal resolution designed to isolate errors associated solely with the nesting procedure, such as those arising from the lateral boundary condition treatment (i.e., the "irreducible error").

The horizontal resolution of $1/48°$ (i.e., approximately 2 km) used in the "truth" and child experiments can be considered at a so-called "gray zone" for resolving mesoscale eddies in the Adriatic Sea. This can be understood through the first baroclinic Rossby radius of deformation (Rd). This key parameter, associated with the spatial scales of baroclinic instabilities (Ferrari & Wunsch, 2009), is commonly used to distinguish between eddy-permitting and eddy-resolving ocean models (Hallberg, 2013; Hurlburt et al., 2008). A fundamental length scale that accounts for the effects of rotation and stratification in a fluid, Rd varies depending on local density properties and latitude. It is expressed as $Rd = \frac{NH}{f}$ where N is the Brunt-Väisälä frequency, H represents the vertical scale of motion, and f is the Coriolis parameter.

The spatial and temporal distribution of Rd in the Adriatic Sea was estimated based on the "truth" experiment outputs. In agreement with what the literature on the Mediterranean Sea proposes, Rd on average varies from 5 to 12 km in the open Mediterranean Sea (Grilli & Pinardi, 1998; Pinardi & Masetti, 2000) but reduces considerably in the vicinity of shallow basins such as the Northern Adriatic, reaching 3–4 km in summer and 1 km in winter (Bergamasco et al., 1996; Cushman-Roisin et al., 2007; Masina & Pinardi, 1994; Paschini et al., 1993; Pranić et al., 2023).

Figure 3 highlights the significant seasonal variability of Rd, particularly in the northern sub-basin, where stratification of the shallow waters vary significantly between summer and winter seasons. During winter, the Northern Adriatic experiences vertically mixed conditions with Rd frequently around 1 km in agreement with Pranić et al. (2023), requiring sub-kilometer resolution to fully resolve mesoscale eddies. In contrast, the summer period is characterized by a stratified water column and larger Rd values reaching 6 km, making a 2 km (i.e., $1/48°$) grid eddy resolving. These variations imply that the ability of the 2 km simulation to represent mesoscale dynamics is strongly season-dependent: under winter conditions, it cannot be considered eddy resolving and is only marginally eddy permitting, meaning that the smallest mesoscale features associated with dense water spreading may be under-resolved. Nevertheless, the 2 km configuration is appropriate for this study, as it reproduces the seasonal to interannual variability of basin-wide thermohaline properties and enables a meaningful comparison of the eddy kinetic energy spectrum and the main features of dense water formation in the Adriatic Sea within a perfect model framework.

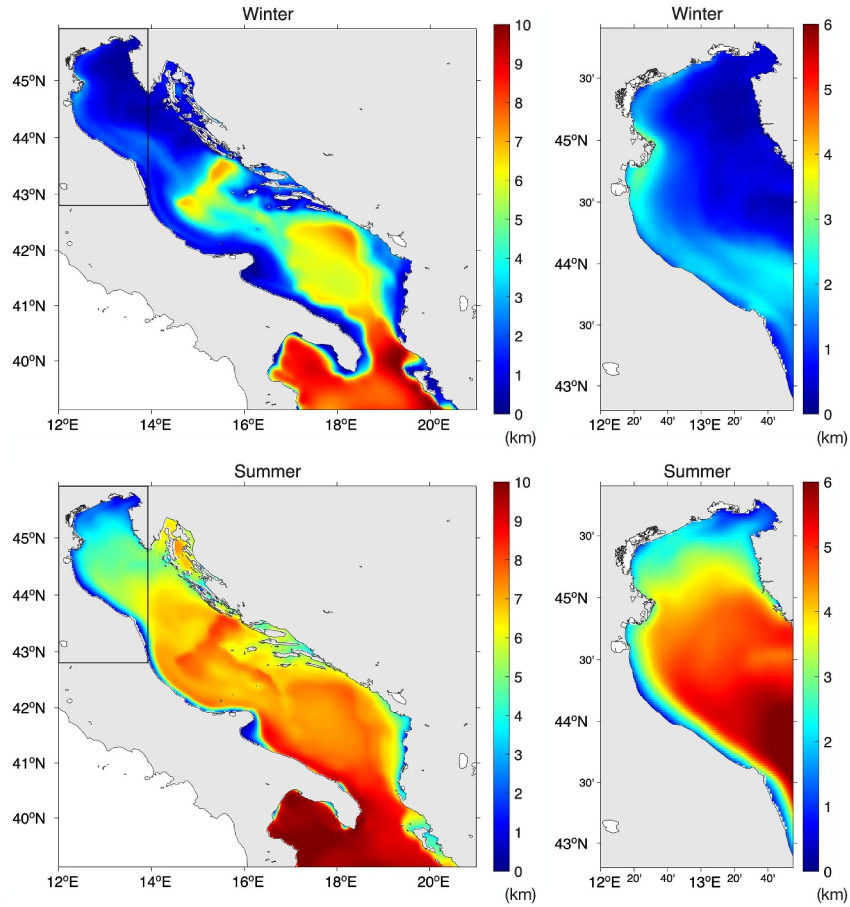

Figure 3. First baroclinic Rossby radius of deformation (km) for Winter (top figures) and Summer (bottom figures) calculated based on the L2 outputs for the Adriatic Sea. Panels on the right correspond to the Northern Adriatic downscaling domain with updated color bar to enhance local characteristics.

3. Reproducibility of Energy Spectra

Power spectral density (PSD) analyses of the eddy kinetic energy (EKE) were performed for all parent and child experiments. Seasonal maps of surface currents were estimated from the "best nesting" child experiment, as shown in Figure 4, and are used to define the optimal area to perform the energy spectrum analysis in the Northern sub-basin. The section along 13.3°E was selected because it captures the inflow along the northeastern shelf, the outflow along the southwestern shelf, and the Northern Adriatic cyclonic gyre, while being far enough from the lateral open boundary to avoid instabilities.

The EKE spectrum was computed using two approaches: in the spatial domain (wavenumber) where PSD was calculated along the meridional transect for each day and in the temporal domain (frequency) where PSD was computed over time for each grid point of the transect. The PSD analysis was applied to the eddy velocity components (u', v'), providing the EKE and revealing the energy distribution on different scales. This approach allows for the inference of EKE spectral characteristics without directly computing the PSD of squared velocities, which can introduce complexity due to nonlinearities. The spectral analysis follows a similar approach of Katavouta and Thompson (2016) with the detailed steps provided in Appendix A.

Figure 5 shows the wavenumber spectrum of EKE for the surface (left panel) and depth averaged (right panel) fields. The agreement between S2 and "truth" L2 confirms the proper setting of the downscaling strategy with minimal error associated to the numerical schemes of the lateral boundary conditions. Moreover, all the downscaling experiments consistently produced higher energy across all wavelengths compared to their parent experiments though their performance varied.

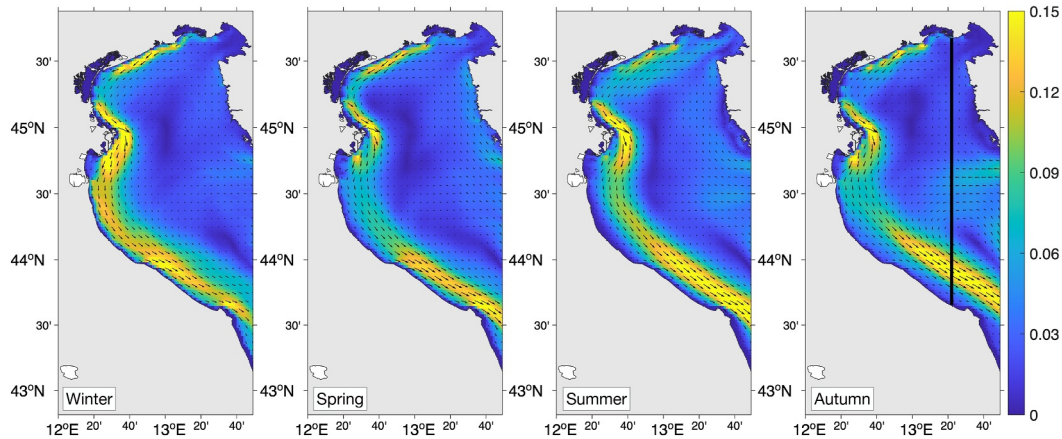

Figure 4. Seasonal surface currents velocity $[\mathrm{m\,s^{-1}}]$ for the S0 experiment. The black line in the right panel indicates the position of transect along longitude 13.3°E used for the spectral analysis.

The S10 (1:5 ratio) experiment mostly overestimated energy relative to the reference solution ("truth" L2) both at surface and depth despite the low energy in its parent experiment, L10. In contrast, S6 (1:3 ratio) performed significantly better with energy levels closely aligning with "truth" L2. The S2F experiment, downscaled from the filtered solution L2F, demonstrates the closest agreement with the "truth" L2 at the surface and does not present energy overshooting at any level. This can be attributed to the low-pass filter's capability to preserve the backward influence of cross-scale processes on large scales. This experiment S2F, however, underestimates depth average EKE at low wavelength.

Similarly, Figure 6 presents the frequency spectrum of EKE for the surface (left panel) and depth averaged (right panel) fields. Unlike the space domain analysis (Figure 5) where energy continuously decreased toward smaller scales, distinct energy peaks are evident in the time domain (Figure 6), each associated with specific events. Downscaled experiments consistently showed higher EKE than their parent experiments reflecting their ability to regenerate the multiscale features. However, the degree of energy recovery varied depending on the nesting strategy and across the different frequency ranges.

The S6 experiment shows again a good agreement with "truth" L2, particularly at the surface, and proves that a 1:3 downscaling ratio effectively regenerates inner-domain EKE. At depth, S6 slightly underestimated (overestimate) energy at the 6-month (4-month) peak. The L6-to-S6 nesting strategy outperforms the L10-to-S10 one and performs comparably to the L2F-to-S2F approach.

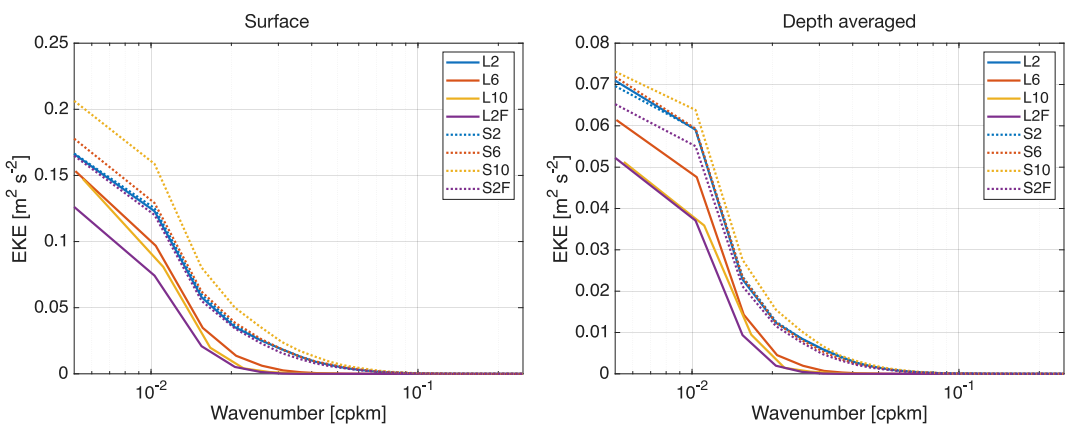

Figure 5. Eddy kinetic energy power spectrum in the wavenumber domain (cycles per km), computed from surface (left) and depth-averaged (right) velocities. Solid and dashed lines indicate the parent and child experiments, respectively; colors represent the nesting strategy. The computation was performed along a longitudinal transect at 13.3°E.

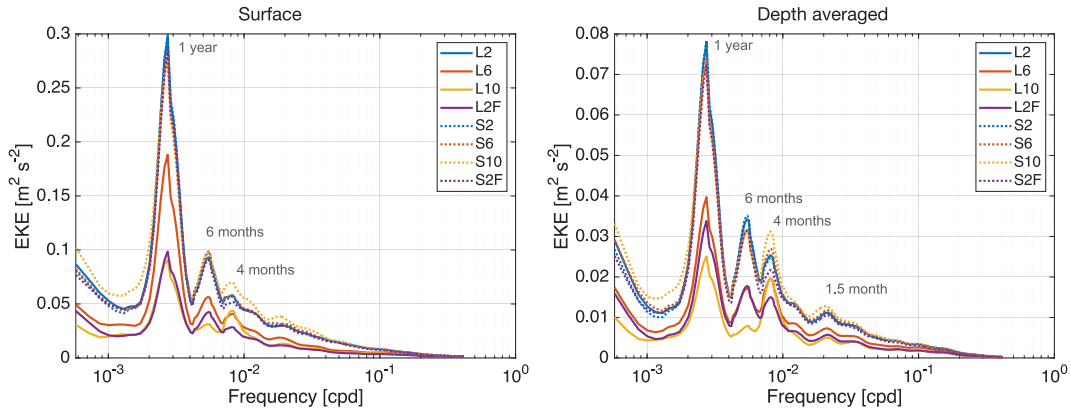

Figure 6. Eddy kinetic energy power spectrum in the frequency domain (cycles per day) computed from surface (left) and depth-averaged (right) velocities. Solid and dashed lines indicate the parent and child experiments, respectively; colors represent the nesting strategy. The computation was performed along a longitudinal transect at 13.3°E.

The S2F experiment demonstrates the effectiveness of downscaling when large-scale patterns introduced at the lateral open boundary incorporate the feedback of cross-scale processes. This feedback is ensured by the low-pass filtering applied in the parent experiment, L2F. Despite the strongly smoothed boundary fields, the S2F experiment successfully regenerated multiscale energy without overshooting, maintaining consistency with the features of the "truth" L2 reference.

In contrast, the S10 experiment exhibited significant overshooting at frequencies shorter than 4 months driven by the coarse resolution of the driving fields. This indicates that a 1:5 downscaling ratio is more prone to introducing spectral inconsistencies from a coarse dynamical parent model. It also highlights the challenge of parameterizing subgrid processes and their impact on larger scales within the coarse-resolution parent experiment (L10), which subsequently affects the lateral open boundary of S10.

Maps of the power spectrum are presented in Appendix B1 to provide additional detail and support the interpretation of the dominant energy peaks as well as their reproducibility across the different experiments. Although it is challenging to isolate features associated with specific frequencies, the seasonal cycle of the northeastern inflow and southwestern outflow, linked to the basin-wide anticlockwise circulation in the Adriatic Sea, is clearly reproduced by all downscaling experiments.

The 6-month and 1-year frequencies reflect the seasonal variability of both the large-scale circulation and specific mesoscale features in the northern sub-basin driven by atmospheric forcing and Po River discharge. The spectral analyses of wind and salinity (provided in Appendix B) align with the observed EKE patterns in the frequency domain (Figure 6). Notably, the wind speed PSD reveals distinct peaks at 1 year, 6 months, and 4 months consistent with the EKE spectrum. Similarly, the salinity spectrum is dominated by 1-year and 6-month peaks, reflecting the seasonality of the Po River and evaporation rate. The 4-month timescale may reflect the development and/or strengthening of the Northern Adriatic cyclonic gyre, which typically lasts for several months, modulated by wind forcing, stratification, and river discharge (Artegiani et al., 1997a; Bergamasco et al., 1996; Cushman-Roisin et al., 2007; Paschini et al., 1993).

At the 4-month peak, the strong influence of boundary forcing becomes more evident, revealing a complex interaction between boundary fields and local processes (atmospheric conditions and rivers). For the S2F case, strongly filtered boundary forcing smooths out mesoscale variability and prevents the nested model from reproducing the correct amount of EKE at this frequency. In contrast, in the S10 configuration, nesting from a coarse dynamical model at a 1:5 downscaling ratio introduces dynamical inconsistencies due to the transition between grids. Moreover, the child domain can explicitly resolve the smaller scales, which were unresolved by the coarse parent L10. This spectral mismatch can generate spurious pressure gradients and unrealistic near-boundary acceleration leading to an artificial amplification of the local circulation.

The overshooting observed in the S10 EKE spectrum can be associated with two complementary, conceptual mechanisms acting at different scales. Near the boundary, the coarse L10 parent provides energy at smaller

unresolved scales that is inconsistent with the local dynamics the child can resolve, leading to an accumulation of energy at larger scales. This interpretation is supported by the EKE maps of spectrum (Figure B1), which show that the overshooting occurs predominantly at scales associated with near-boundary features. Within the child domain, the higher resolution allows explicit representation of multiscale motions, and energy may be explicitly redistributed through direct and inverse cascades. However, as hinted by the 4-month peak and the overestimation at the smaller frequencies/wavenumbers, near-boundary recirculation combined with the inconsistent energy input from the parent model may inhibit the normal redistribution pathways, allowing energy to accumulate at larger wavelengths.

This modeling outcome hints at the sensitivity of coarser-resolution experiments to subgrid parameterizations, as they neglect a wide range of turbulent eddies that drive both direct and inverse energy cascades at lower wave numbers. The parent experiment L10 contains higher EKE than L2F, which is transferred into its downscaled child S10, amplifying energy at the inner domain and leading to overshooting. L2F, in contrast, maintains a more realistic representation of the large-scale geostrophic turbulence, as it inherits the dynamically consistent flow field explicitly resolved by L2, thereby preventing overshooting in S2F despite following a downscaling ratio comparable to S10.

In the frequency domain it is evident that the S10 overshooting affects the power spectrum mostly at lower frequencies and the 4-month peak, which are a result of the EKE entering at the lateral open boundaries. In contrast, the peaks at 1 year and 6 months periods, which reflect the local atmospheric patterns and Po River runoff regime, are reproduced as accurately as in the other downscaled experiments. This indicates that the seasonal and interannual variability driven by local processes have no strong effect from the parent model fields at the open ocean boundary.

Maps of currents from the upper 15 m (Figure 7) indicate the flow pattern in summer (July) and autumn/winter (November) of 2012 for each downscaling experiment compared with the reference L2 (restricted to the Northern Adriatic sub-domain). The year 2012 was selected as it highlights the differences among the experiments and is also characterized for the occurrence of a large dense water formation event and strong Bora wind episodes (Cushman-Roisin et al., 2013; Janeković et al., 2014; Mihanović et al., 2013; Vilibić et al., 2016).

The results show clear seasonal variability in the Northern Adriatic circulation with a stronger western current along the Italian coast in summer. A double gyre configuration is evident with the main Northern Adriatic cyclonic gyre and a secondary cyclonic gyre in the northern part of the basin; this secondary gyre intensifies in summer consistent with observations by Poulain (2001). These primary features are reproduced by all downscaling experiments though with some differences mostly in strength. As expected, S2 shows the closest match to the reference L2. S6 shows slight deviations but is able to reproduce the main flow features well, indicating that the nesting effectively captures the circulation.

In experiment S10, the overshooting observed in the EKE analysis is particularly evident with the main gyre currents stronger than in the reference L2 and other nested simulations. This behavior is consistent with the idea that the child model receives unbalanced or misrepresented energy at smaller unresolved scales through the coarse L10 boundaries, and that internal nonlinear interactions cannot fully redistribute it. As a result, energy may accumulate at larger scales, leading to overshooting in the EKE maps and spectra.

The parent forcing L2F suppresses mesoscale variability at the boundaries, producing a slightly smoother near-boundary circulation in the child S2F, yet the overall circulation remains largely comparable to the truth L2. Despite the large downscaling ratio (∼1:5) and modest reductions in kinetic energy at specific wavelengths, S2F still preserves realistic distribution of energy across scales. These results indicate that effective downscaling depends not only on the downscaling ratio but also on the spectral consistency of the parent fields. For dynamical parents, where the imprint of smaller-scale dynamics is absent, a 1:3 ratio avoids the scale mismatches and overshooting seen in the 1:5 case (S10). In contrast, when the parent fields retain large-scale structures shaped by smaller-scale dynamics, as in the filtered L2F case, the child model (S2F) can recover realistic dynamics even with a 1:5 ratio.

The overall recovery of energy across all downscaling strategies highlights the dominance of local drivers in Northern Adriatic variability. On the other hand, the limitations encountered by the downscaling experiments at specific frequencies and also in wavenumber hint that accurate EKE recovery by the nested experiment depends on the consistency of the large scale patterns entering through the lateral open boundary. Altogether, these results

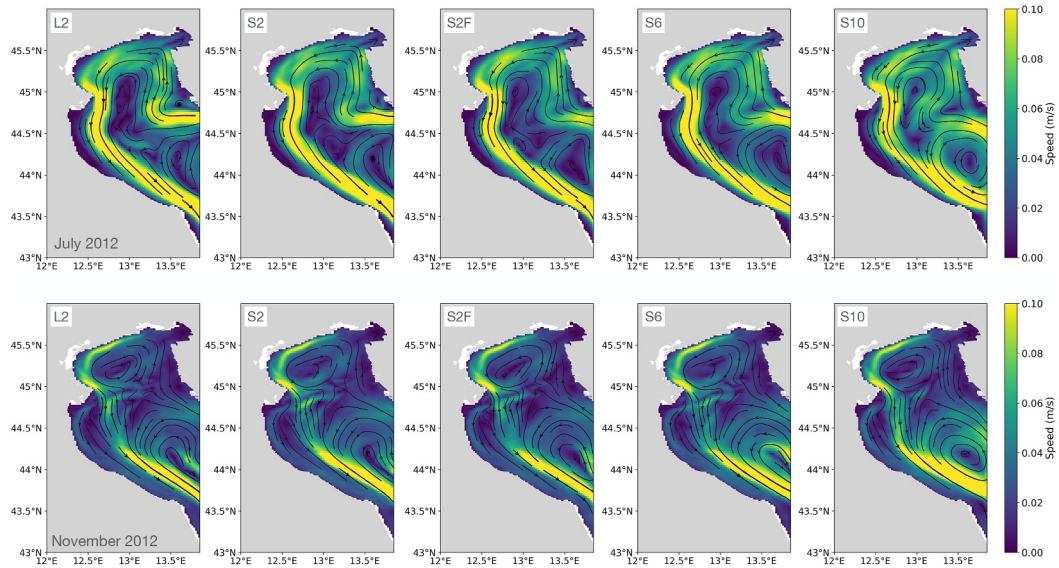

Figure 7. Mean current speed in the upper 15 m for summer (July)—top panels, and autumn/winter (November)—bottom panels, 2012, for the reference experiment L2 and the downscaling experiments.

demonstrate that an optimal downscaling strategy and resolution ratio should therefore preserve spectral continuity across the boundary, ensuring that the nested model can develop realistic mesoscale variability without introducing artificial energy amplification.

4. Reproducibility of Dense Water Formation

The dense water formation in the Northern Adriatic sub-basin is examined using estimates of the volume of water with a potential density anomaly (PDA) that exceeds a threshold value of $\sigma_t > 29.2$ kg m^{-3} as suggested previous studies (Artegiani et al., 1997a; Janeković et al., 2014; Vilibić et al., 2016). Figure 8 represents dense water volume (top panel), temperature (middle panel), and salinity (bottom panel) in this sub-basin computed for each of the different downscaling experiments and the "truth" L2.

There is a clear seasonal variability in the thermohaline properties primarily driven by winter cooling, especially during Bora wind events (Cushman-Roisin et al., 2013; Vilibić & Supić, 2005). The increase in dense water volume as a result of heat loss is mostly evident in 2002–2012. During this period, there is good agreement between the child experiments and the "truth" L2, highlighting the ability of the downscaling to reproduce the dense water dynamics when local drivers dominate. Specifically, in 2012, exceptional Bora wind conditions combined with extremely low winter temperatures led to a well known increase in dense water formation in the Adriatic Sea (Cushman-Roisin et al., 2013; Janeković et al., 2014; Mihanović et al., 2013; Vilibić et al., 2016). This anomalous year, marked by extreme atmospheric conditions, was well captured by all downscaling experiments, including those with coarser parent solutions (e.g., L10 to S10).

After 2012, the dense water volume decreases significantly in the "truth" L2. For this period, the downscaling experiments failed to simulate the dense water volume correspondent to L2 with the exception of S2F. Although S2F accurately reproduces the local thermohaline properties, in S6 and S10 the dense water is colder and fresher compared to L2, indicating that remote drivers, not adequately represented in the coarse parent models, are influencing the dense water formation during this period. The performance of S2F emphasizes that, after 2012, reproducibility of dense water formation by the downscaling experiments depends on accurately capturing large-scale ocean patterns entering the lateral boundary rather than the choice of downscaling ratio.

The temperature and salinity variability of the Northern Adriatic dense water is influenced by both local and remote drivers across different timescales (Vilibić et al., 2020). Local drivers include the river runoff and net heat flux, whereas remote drivers were found to be mostly associated with the circulation regime of the Ionian Sea. Notably, after 2012, a shift in the NIG is identified as a possible driver of thermohaline variability in the region.

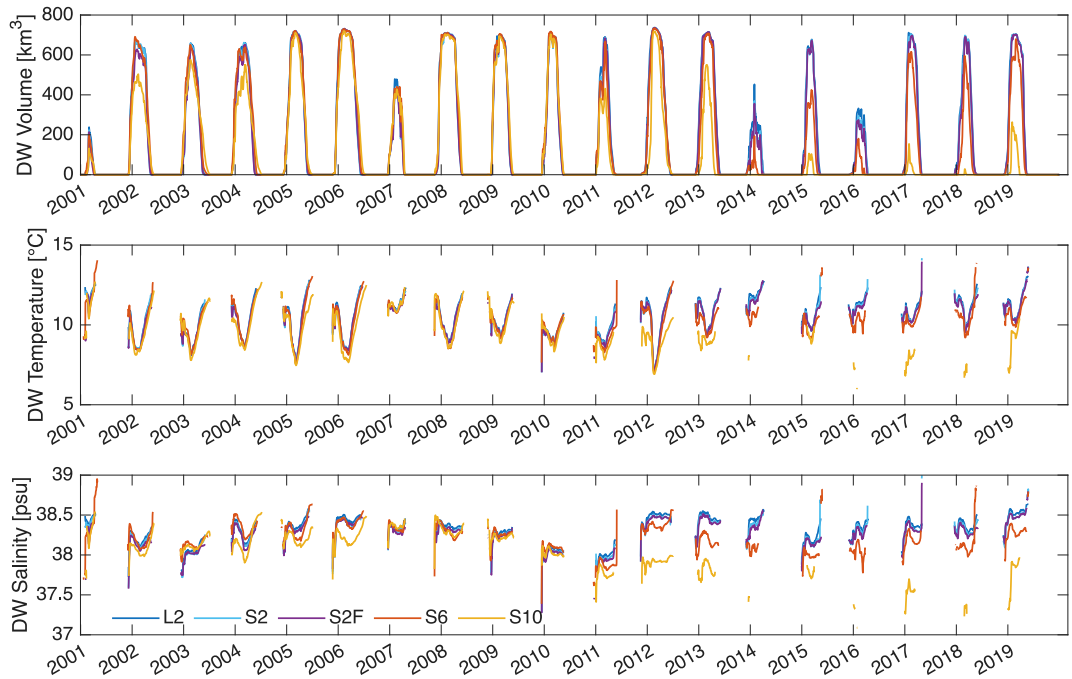

Figure 8. Dense water volume (top), dense water temperature (middle), and dense water salinity (bottom) for each downscaling experiment and the reference L2, computed within the region of the Northern Adriatic nesting domain.

This shift can be attributed to the BiOS cyclonic phase where the NIG rotates counterclockwise, facilitating the intrusion of eastern saltier and warmer waters formed at intermediate depths in the Levantine Basin, known as Levantine Intermediate Water (LIW). This increases the salinity in the inner Adriatic and promotes water sinking and dense water formation especially in the southern sub-domain.

Figure 9 shows the salinity maps at the sea surface (top panels) and at a typical depth of the LIW inflow, that is, 150 m depth (middle panels), illustrating the LIW entering the Adriatic Sea during the BiOS cyclonic phase. This is mostly evident in the "truth" L2 and L2F experiments where this saltier water mass is being advected northward. The reproducibility of dense water volume in the downscaling experiments during this period depended largely on the accuracy of the parent large-scale driving fields, which were well-captured in the S2 and S2F experiments. In contrast, dense water was underestimated in the S6 and S10 experiments due to limitations in their parent models, L6 and L10, respectively. The coarse resolution of these parent models constrained the intrusion of LIW through the Otranto Strait, limiting the northward propagation of this water into the Adriatic Sea.

The bottom panels in Figure 9 show the vertical profile of salinity along a latitudinal transect at the Otranto Strait (40.2°N), where the water exchange is dominated by inflow on the eastern side and outflow on the western side (Ferentinos & Kastanos, 1988; Zavatarelli & Pinardi, 2003). A single day at the beginning of summer 2012 was chosen to illustrate the reproducibility of this feature across experiments. The full sequence of daily salinity maps at 150 m depth for 2012 is provided as Movies S1–S4, illustrating the signature of the saltier LIW across the different parent experiments.

The expected inflow of saltier water at mid-depths along the eastern side is evident in the reference simulation (L2), and its associated large-scale circulation pattern is retained in the filtered version (L2F). In contrast, the parent experiments L6 and especially L10 fail to capture the correct water exchange through the Otranto Strait. Although the transect at 40.2°N is sampled by a non-negligible number of surface grid points (49 in L2, 16 in L6, and 8 in L10), the 6–10 km configurations cannot reproduce the correct inflow-outflow structure. This suggests that, although the model configurations are able to represent the strait by a few up to several tens of grid points and the Rossby radius is at least comparable to the horizontal resolution (Figure 3), local processes such as shear, turbulence, and cross-scale interactions could play a role in shaping the water exchange, which remain under-resolved at coarser resolutions. The L2F experiment, however, preserves the influence from this water

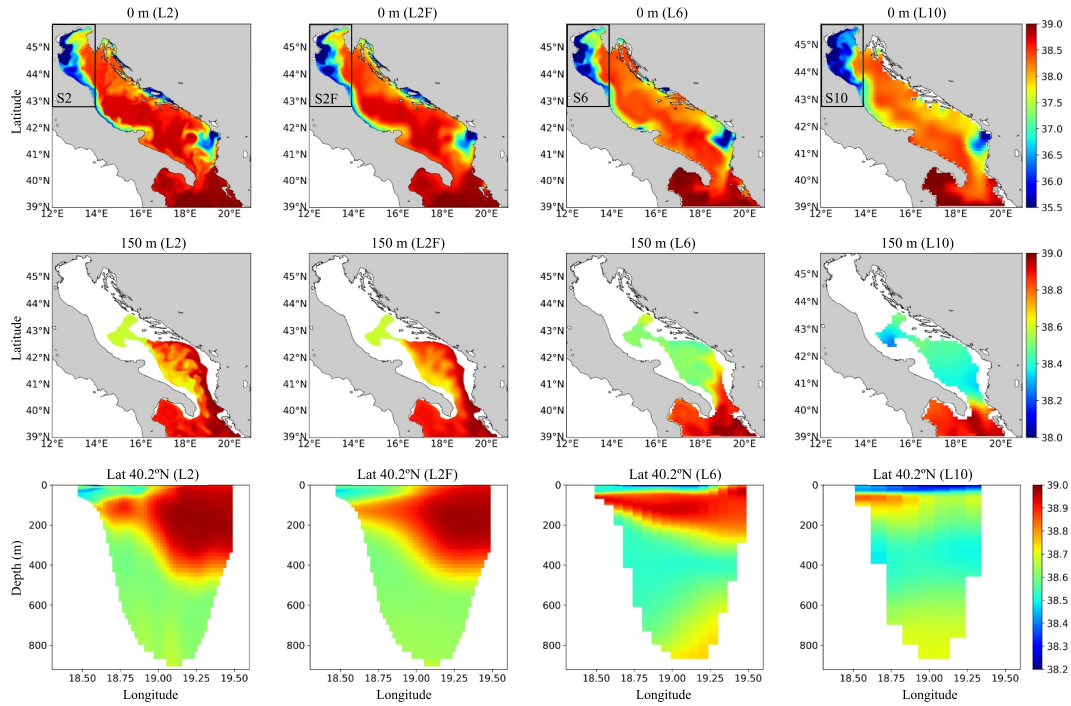

Figure 9. Salinity (psu) at surface (top panels) and 150 m depth (middle panels), and along a vertical section at the Otranto Strait at 40.2°N, for the parent models and their respective downscaled experiment on 21/06/2012. The color scale has been adjusted to highlight depth-dependent salinity variations.

exchange, as it reflects large-scale patterns that have already been shaped by cross-scale interactions in the original high-resolution simulation.

The strong underestimation of cross-strait exchange in the coarse parent dynamical experiments compared with the reference "truth" reflect limitations specific to low resolution configurations in numerical modeling. Particularly, the 6–10 km grids cannot adequately resolve the vertical and lateral structure of the Otranto Strait exchange, compromising the representation of a realistic horizontal two-layer system over depth (western outflow coupled with eastern inflow) and the associated vertical anti-estuarine circulation. Moreover, the combination of coarser resolution and enhanced mixing, associated with the parameterization of unresolved scales, can affect the model's ability to advect salty waters into the basin, a limitation also noted by Oddo and Guarnieri (2011), who linked excessive mixing to the underestimation of the LIW intrusion into the Adriatic. In addition, as discussed in the analysis of the EKE power spectra, the coarser-resolution experiments are highly sensitive to subgrid parameterizations and they neglect energy transferred from the smaller scales to the larger scales thus preventing a realistic representation of the lateral turbulent fluxes.

To provide a broader perspective on the reproducibility of dense water formation, Table 2 summarizes mean differences (bias and RMSD) of February monthly mean bottom PDA between the downscaling experiments and the reference L2 for key dense water years (2006, 2009, 2012, 2013, 2017, and 2019). Overall, S2 and S2F exhibit the smallest deviations with RMSD around 0.05–0.06 kg/m^3. S6 shows good agreement in the early years, indicating that the downscaling strategy is sufficient to reproduce bottom PDA during major events under local driving forces. After the BiOS inversion to cyclonic phase around 2012, however, when parent L6 fails to capture the entrance of saltier waters, local density properties deviate from the reference L2, leading to higher RMSD and predominantly negative biases. In contrast, S10 already underperforms in the initial years, reflecting the difficulty of reproducing the local features under a high downscaling ratio (1:5) with too coarse parent solution. This limitation becomes more pronounced after the BiOS inversion, when both RMSD and biases increase substantially.

Despite the dominant role of local heat fluxes in modulating dense water formation within the Northern Adriatic, the results reinforce the importance of realistically representing boundary exchanges and salinity inflows. Pranić

Table 2
Mean February Bottom PDA Differences (Bias/RMSD) for Selected Dense Water Formation Years, Basin-Averaged Over the Northern Adriatic Sub-Domain, for Each Downscaling Experiment Relative to the Reference L2

Experiment	2006	2009	2012	2013	2017	2019
S2	−0.03/0.05	−0.03/0.05	−0.03/0.04	−0.02/0.03	−0.02/0.05	−0.03/0.05
S6	0.00/0.11	0.02/0.10	−0.09/0.16	−0.16/0.20	−0.17/0.24	−0.19/0.24
S10	−0.13/0.29	−0.02/0.19	−0.45/0.49	−0.40/0.42	−0.59/0.61	−0.64/0.68
S2F	−0.02/0.06	−0.03/0.06	−0.04/0.06	−0.02/0.05	−0.03/0.07	−0.03/0.06

Note. Units are kg/m^3.

et al. (2023) demonstrated that outdated river climatologies in ocean models can reduce salinity and lead to underestimated dense water generation. Here, the role of remote influences, particularly the inflow of saltier waters through the Otranto Strait modulated by the BiOS, emerge as a key factor in salinity intrusion with cascading effects in the precondition of dense water formation. Although previous studies have linked the BiOS regime with changes in salinity and density (Vilibić et al., 2020), its specific role in the Northern Adriatic dense water formation had not been fully explored. The present results thus provide new insights into its contribution on dense water through remote salt intrusion effects.

5. Summary and Conclusions

Using a "perfect model" approach, the performance of dynamical downscaling in the Northern Adriatic Sea was assessed in terms of its ability to regenerate the small-scale features and reproduce local physical processes. A high-resolution multidecadal simulation covering the entire Adriatic Sea served as the reference "truth" for comparison with a series of one-way nested experiments, each reaching the same horizontal resolution (2 km) within the Northern Adriatic sub-basin. The downscaling experiments differed in their parent driving fields, which followed two approaches: a statistically generated parent obtained by low-pass filtering the reference experiment, that is, using the "truth" large scales; and low resolution numerical experiments, that is, representing coarse model estimated large scales.

Analysis of Eddy Kinetic Energy (EKE) revealed that the experiment downscaled from the 6 km parent model closely reproduces the EKE power spectrum of the "truth" experiment. This indicates that the downscaling ratio of 1:3 effectively captures the local energy budget and recovers the energy distribution across spatial and temporal scales. On the other hand, the child experiment downscaled from the 10 km parent model exhibited significant overshooting at specific frequencies and wavelengths, demonstrating that large resolution ratios (1:5) are more prone to energy imbalances. In this case, the child receives inconsistent or misrepresented energy at smaller unresolved scales through the boundaries, and the internal nonlinear redistribution cannot fully redistribute it, allowing energy to accumulate at specific larger scales not feeding the forward energy cascade.

The filtered "truth" parent experiment, designed to extract the large-scale features (∼10 km) from the full reference experiment, improved EKE recovery through the nesting strategy, outperforming the downscaling from 10 km grid parent model. This improvement arises because, unlike the dynamical parent models at 6 and 10 km, which evolve independently at their resolution, the statistically generated filtered "truth" parent preserves accurate large scales that have been shaped by the small scales. This demonstrates that although a 1:3 ratio is a robust choice for dynamical downscaling from coarse parents, larger ratios (e.g., 1:5) can be effective when the parent boundary fields are spectrally consistent and retain the imprint of small-scale processes.

The critical role of cross-scale interactions in shaping the Adriatic dynamics are highlighted not only by the spectral analysis of EKE but also the multiannual variability in dense water formation. When local processes, such as buoyancy fluxes, dominate, dense water formation in the Northern Adriatic is well reproduced by all downscaling experiments with seasonal and interannual variability following winter cooling and wind-driven heat loss. However, when remote influences become dominant particularly the intrusion of Levantine Intermediate Water (LIW) during the cyclonic phase of the Adriatic-Ionian Bimodal Oscillation System (BiOS), the ability of the experiments to reproduce dense water formation strongly depends on the accuracy of the parent model's large-scale fields. Limitations were evident in child experiments nested within the coarser 6 and 10 km parent

models, which failed to reproduce the key salinity intrusions. In contrast, the filtered "truth" parent, which preserved large-scale fields originally shaped by fine-scale dynamics, enabled better representation of remote forcings in the nested experiment.

Results show that, when modeling the Adriatic Sea, a 6 km horizontal resolution is insufficient to capture the LIW inflow through the Otranto Strait, as the small-scale and mesoscale processes that contribute to water exchange remain under-resolved. An accurate representation of the strait dynamics requires a finer horizontal resolution even though the bathymetry is considerably deep and the local Rossby radius of deformation is relatively large. A 2 km horizontal resolution is found to be suitable to capture mesoscale dynamics and the cross-scale processes driving water exchange through the strait with cascading effect on the thermohaline properties and dense water formation of the Northern Adriatic sub-basin. The filtered "truth" parent carries memory of these interactions, which then enter the downscaled experiment in the Northern Adriatic through the lateral boundaries, enhancing the reproducibility of dense water formation when compared with child experiments nested into coarse dynamical models (6–10 km).

The outcomes of this work demonstrate that effective downscaling depends not only on the nested model's configuration and ability to reproduce local small-scale processes but also on the consistency of the parent model's large-scale dynamics entering at the lateral open boundaries, which improves when cross-scale interactions are preserved in the driving fields. For the Adriatic, the study provides insights into basin thermohaline circulation, emphasizing the dual importance of local and remote drivers for dense water formation in the northern sub-basin. Additionally, the observed multiannual variability, together with differences across downscaling approaches, further highlights the potential impact of the BiOS on dense water formation in the Northern Adriatic Sea.

The Adriatic case highlights some of the challenges in modeling marginal seas, particularly in strait systems where limited resolution and inaccurate boundary inflows can misrepresent salinity pathways. More broadly, the findings have implications for coastal downscaling efforts in other regions with complex geometries where straits exert strong control on basin thermohaline properties (e.g., the Strait of Gibraltar, the Bosphorus Strait, and the Indonesian Throughflow). In such systems, one-way nesting strategies, grid-spacing, and mixing parameterizations must be carefully designed to capture strait dynamics and avoid underestimation of water exchanges that drive water mass transformation. Moreover, large resolution ratios in downscaling should be used with caution, as coarse parent models can misrepresent energy transfers, potentially generating spurious currents or distortions in the child energy spectrum.

The "perfect model" approach proved valuable for establishing a downscaling modeling chain that effectively balances computational cost with capability to solve multiscale processes. This study finally provides directions for further investigations in the framework of coastal climate downscaling, including two-way nesting, adaptive horizontal resolution, and spatially variable locally tailored turbulence closure schemes.

Appendix A: Power Spectrum Density Computation

The power spectrum density (PSD) analysis applied to the velocity components (u, v) leading to EKE, followed these steps:

1. Removal of time and space mean of u and v, resulting in eddy velocities (u', v');
2. Application of a windowing function (Hanning window (Oppenheim, 1999)) to minimize spectral leakage;
3. Fast Fourier Transform (FFT, Frigo & Johnson, 2005) to decompose the signal into frequency (or wavenumber) components. The transforms are defined as $Y(k) = \sum_{j=1}^{n} X(j) W_n^{(j-1)(k-1)}$ where W_n is the root of unity $W_n = e^{\frac{-2\pi i}{n}}$;
4. Computation of PSD for time (or spatial) intervals by multiplying the amplitude of the FFT by its conjugate and normalize it to the frequency (or wavelength) of the bin width. Time interval for the frequency analysis will be the time frequency of the model output, that is, days, whereas the space interval in the wavelength analysis is the respective grid spacing of each experiment (i.e., 2, 6, and 10 km);
5. Window correction to account for energy loss in step 2;
6. Smoothing of the spectrum for statistical robustness in the frequency domain analysis;
7. Averaging in time (for wavenumber analysis) or space (for frequency analysis).

Appendix B: Complementary Spectral Analysis

B1. Maps of Spectrum

Figure B1 shows spectral maps for energy peaks at frequencies of 4 months, 6 months, and 1 year. These maps highlight the spatial distribution of EKE variability associated with each peak and the differences between experiments particularly the ability of the downscaling experiments (middle panels) to reproduce features comparable to "truth" L2 (left panels).

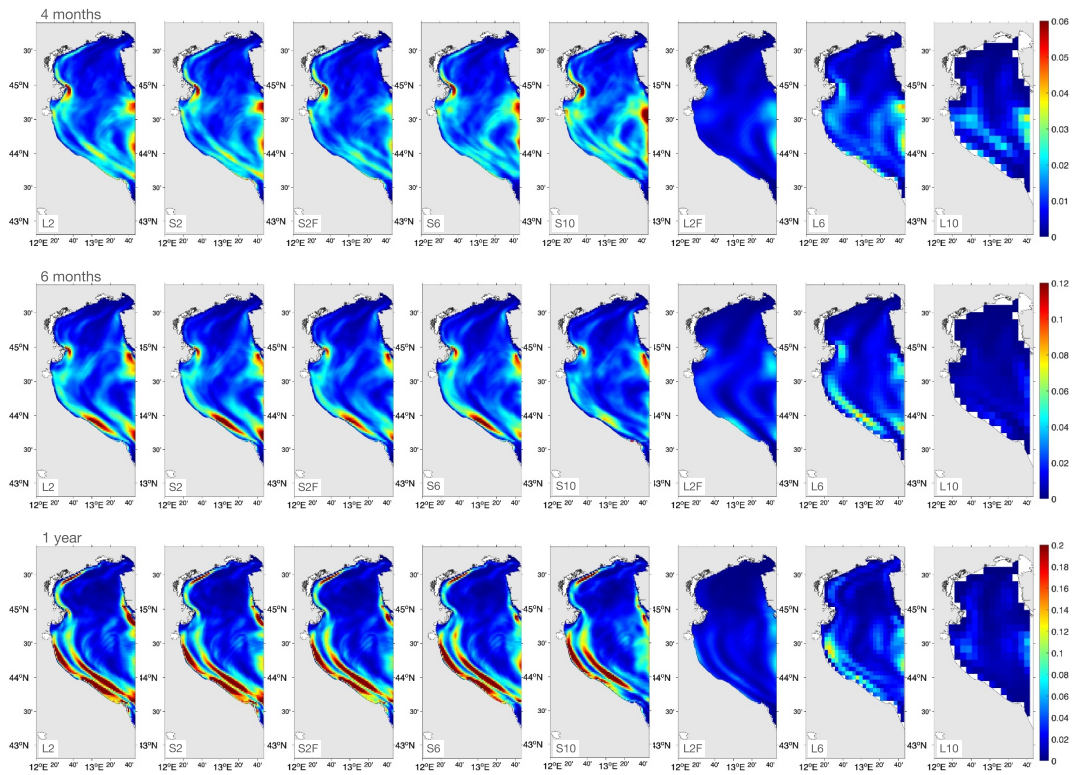

Figure B1. EKE spectrum $\left[m^2\ s^{-2}\right]$ for the "truth" L2 (left), the downscaling experiments S2, S2F, S6, and S10, and their respective parent models L2F, L6, and L10, at 4-month (top), 6-month (middle), and 1-year (bottom) frequencies. The color scale is adjusted for each frequency to emphasize differences between experiments. The L2 and parent experiment domains are subset to the Northern Adriatic (child domain). Depth-averaged fields are used in the analysis.

B2. Spectrum of Winds and Salinity

Figure B2 shows the power spectral density of wind velocity components (left panel) and salinity field (right panel). In both cases, the dominant peaks at 1-year and 6-month frequencies account for most of the regional variability. Salinity in the Northern Adriatic primarily reflects the seasonality of the Po River discharge and evaporation rate. For the wind field, additional higher-frequency peaks are observed similar to those previously identified in the EKE spectrum. This suggests that EKE variability is largely driven by atmospheric forcing.

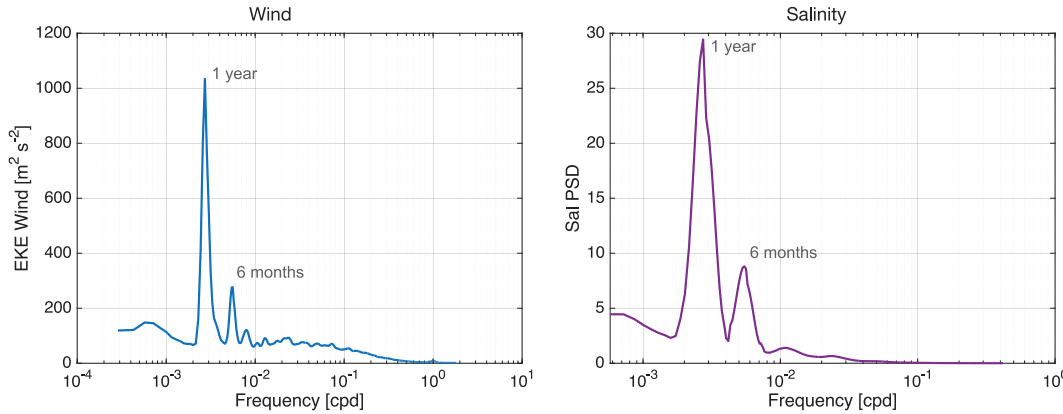

Figure B2. Power spectral density (PSD) in the frequency domain (cycles per day): (left) PSD of wind velocity components leading to EKE, averaged over the Northern Adriatic sub-domain; (right) PSD of depth-averaged salinity for the S2 experiment along a longitudinal transect at 13.3°E.

Conflict of Interest

The authors declare no conflicts of interest relevant to this study.

Data Availability Statement

Supporting data and files for this article, including selected model outputs, analysis scripts, and codes, are publicly available on Zenodo at https://doi.org/10.5281/zenodo.17378867.

Acknowledgments

The authors acknowledge the University of Bologna Ph.D. program "Future earth, climate change and societal challenges" and the financial support provided by the CMCC Foundation (Euro-Mediterranean Center on Climate Change), the Marco Polo mobility program, and the Interreg Italy-Croatia AdriaClimPlus project (ITHR0200333). The FLAME (Future Coastal Ocean Climates) initiative is also acknowledged for its role under the UN Ocean Decade Action within the CoastPredict Program. The model configuration and contributions from V. S. da Costa and G. Verris's were supported by Interreg IT-HR AdriaClim project (ID 10252001) and Spoke 4ICSC-Centro Nazionale di Ricerca in High Performance Computing, Big Data, and Quantum Computing, funded by the European Union-NextGenerationEU (Project PNRR-HPC, CN00000013, CUP: C83C22000560007).

References

Aragão, L., Mentaschi, L., Pinardi, N., Verri, G., Senatore, A., & Di Sabatino, S. (2024). The freshwater discharge into the Adriatic Sea revisited. *Frontiers in Climate*, *6*, 1368456. https://doi.org/10.3389/fclim.2024.1368456

Artegiani, A., Paschini, E., Russo, A., Bregant, D., Raicich, F., & Pinardi, N. (1997a). The Adriatic Sea general circulation. Part I: Air–sea interactions and water mass structure. *Journal of Physical Oceanography*, *27*(8), 1492–1514. https://doi.org/10.1175/1520-0485(1997)027<1492:tasgcp>2.0.co;2

Artegiani, A., Paschini, E., Russo, A., Bregant, D., Raicich, F., & Pinardi, N. (1997b). The Adriatic Sea general circulation. Part II: Baroclinic circulation structure. *Journal of Physical Oceanography*, *27*(8), 1515–1532. https://doi.org/10.1175/1520-0485(1997)027<1515:tasgcp>2.0.co;2

Astraldi, M., Balopoulos, S., Candela, J., Font, J., Gacic, M., Gasparini, G., et al. (1999). The role of straits and channels in understanding the characteristics of Mediterranean circulation. *Progress in Oceanography*, *44*(1–3), 65–108. https://doi.org/10.1016/s0079-6611(99)00021-x

Bergamasco, A., Gačić, M., Boscolo, R., & Umgiesser, G. (1996). Winter oceanographic conditions and water mass balance in the northern Adriatic (February 1993). *Journal of Marine Systems*, *7*(1), 67–94. https://doi.org/10.1016/0924-7963(94)00037-9

Boer, G. J. (2004). Long time-scale potential predictability in an ensemble of coupled climate models. *Climate Dynamics*, *23*(1), 29–44. https://doi.org/10.1007/s00382-004-0419-8

Bonaduce, A., Cipollone, A., Johannessen, J. A., Staneva, J., Raj, R. P., & Aydogdu, A. (2021). Ocean mesoscale variability: A case study on the Mediterranean Sea from a re-analysis perspective. *Frontiers in Earth Science*, *9*, 724879. https://doi.org/10.3389/feart.2021.724879

Castellari, S., Pinardi, N., & Leaman, K. (1998). A model study of air–sea interactions in the Mediterranean Sea. *Journal of Marine Systems*, *18*(1–3), 89–114. https://doi.org/10.1016/s0924-7963(98)90007-0

Chassignet, E. P., Yeager, S. G., Fox-Kemper, B., Bozec, A., Castruccio, F., Danabasoglu, G., et al. (2020). Impact of horizontal resolution on global ocean–sea ice model simulations based on the experimental protocols of the Ocean Model Intercomparison Project Phase 2 (OMIP-2). *Geoscientific Model Development*, *13*(9), 4595–4637. https://doi.org/10.5194/gmd-13-4595-2020

Cushman-Roisin, B., Gacic, M., Poulain, P.-M., & Artegiani, A. (2013). *Physical oceanography of the Adriatic Sea: Past, present and future*. Springer Science & Business Media.

Cushman-Roisin, B., Korotenko, K. A., Galos, C. E., & Dietrich, D. E. (2007). Simulation and characterization of the Adriatic Sea mesoscale variability. *Journal of Geophysical Research*, *112*(C3). https://doi.org/10.1029/2006jc003515

da Costa, V. S., Alessandri, J., Verri, G., Mentaschi, L., Guerra, R., & Pinardi, N. (2024). Marine climate indicators in the Adriatic Sea. *Frontiers in Climate*, *6*, 1449633. https://doi.org/10.3389/fclim.2024.1449633

De Elia, R., Laprise, R., & Denis, B. (2002). Forecasting skill limits of nested, limited-area models: A perfect-model approach. *Monthly Weather Review*, *130*(8), 2006–2023. https://doi.org/10.1175/1520-0493(2002)130<2006:fslonl>2.0.co;2

Denamiel, C., Šepić, J., Ivanković, D., & Vilibić, I. (2019). The Adriatic Sea and coast modelling suite: Evaluation of the meteotsunami forecast component. *Ocean Modelling*, *135*, 71–93. https://doi.org/10.1016/j.ocemod.2019.02.003

Denamiel, C., Tojčić, I., Pranić, P., & Vilibić, I. (2022). Modes of the bios-driven Adriatic Sea thermohaline variability. *Climate Dynamics*, *59*(3), 1097–1113. https://doi.org/10.1007/s00382-022-06178-4

Denamiel, C., Tojčić, I., & Vilibić, I. (2021). Balancing accuracy and efficiency of atmospheric models in the northern Adriatic during severe bora events. *Journal of Geophysical Research: Atmospheres*, *126*(5), e2020JD033516. https://doi.org/10.1029/2020jd033516

Denis, B., Laprise, R., & Caya, D. (2003). Sensitivity of a regional climate model to the resolution of the lateral boundary conditions. *Climate Dynamics*, *20*(2), 107–126. https://doi.org/10.1007/s00382-002-0264-6

Denis, B., Laprise, R., Caya, D., & Côté, J. (2002). Downscaling ability of one-way nested regional climate models: The big-brother experiment. *Climate Dynamics*, *18*(8), 627–646. https://doi.org/10.1007/s00382-001-0201-0

Dominicis, M. D., Falchetti, S., Trotta, F., Pinardi, N., Giacomelli, L., Napolitano, E., et al. (2014). A relocatable ocean model in support of environmental emergencies: The costa Concordia emergency case. *Ocean Dynamics*, *64*(5), 667–688. https://doi.org/10.1007/s10236-014-0705-x

Escudier, R., Clementi, E., Cipollone, A., Pistoia, J., Drudi, M., Grandi, A., et al. (2021). A high resolution reanalysis for the Mediterranean Sea. *Frontiers in Earth Science*, *9*, 702285. https://doi.org/10.3389/feart.2021.702285

Ferentinos, G., & Kastanos, N. (1988). Water circulation patterns in the Otranto straits, Eastern Mediterranean. *Continental Shelf Research*, *8*(9), 1025–1041. https://doi.org/10.1016/0278-4343(88)90037-4

Ferrari, R., & Wunsch, C. (2009). Ocean circulation kinetic energy: Reservoirs, sources, and sinks. *Annual Review of Fluid Mechanics*, *41*(1), 253–282. https://doi.org/10.1146/annurev.fluid.40.111406.102139

Flather, R. (1976). A tidal model of the northwest European Continental shelf. *Mémoires de la Société Royale des Sciences de Liège*, *10*, 141–164.

Fox-Kemper, B., Adcroft, A., Böning, C. W., Chassignet, E. P., Curchitser, E., Danabasoglu, G., et al. (2019). Challenges and prospects in ocean circulation models. *Frontiers in Marine Science*, *6*, 65. https://doi.org/10.3389/fmars.2019.00065

Frigo, M., & Johnson, S. G. (2005). The design and implementation of FFTW3. *Proceedings of the IEEE*, *93*(2), 216–231. https://doi.org/10.1109/jproc.2004.840301

Gačić, M., Borzelli, G. E., Civitarese, G., Cardin, V., & Yari, S. (2010). Can internal processes sustain reversals of the ocean upper circulation? The Ionian sea example. *Geophysical Research Letters*, *37*(9). https://doi.org/10.1029/2010gl043216

Gascard, J. (1978). Mediterranean deep-water formation baroclinic instability and Oceanic eddies. *Oceanologica Acta*, *1*(3), 315–330.

Gaspar, P., Grégoris, Y., & Lefevre, J.-M. (1990). A simple eddy kinetic energy model for simulations of the oceanic vertical mixing: Tests at station papa and long-term upper ocean study site. *Journal of Geophysical Research*, *95*(C9), 16179–16193. https://doi.org/10.1029/jc095ic09p16179

Giordano, F., Querin, S., Reini, M., & Salon, S. (2024). High-resolution modelling of a shallow marginal sea to assess the potential of energy production from marine currents: The northern Adriatic Sea case study. *Bulletin of the Geophysical Observatory*. https://doi.org/10.4430/bgo00466

Grilli, F., & Pinardi, N. (1998). The computation of Rossby radii of deformation for the Mediterranean Sea. *MTP news*, *6*(4), 4–5.

Hallberg, R. (2013). Using a resolution function to regulate parameterizations of oceanic mesoscale eddy effects. *Ocean Modelling*, *72*, 92–103. https://doi.org/10.1016/j.ocemod.2013.08.007

Hersbach, H., Bell, B., Berrisford, P., Hirahara, S., Horányi, A., Muñoz-Sabater, J., et al. (2020). The ERA5 global reanalysis. *Quarterly Journal of the Royal Meteorological Society*, *146*(730), 1999–2049. https://doi.org/10.1002/qj.3803

Hurlburt, H. E., Chassignet, E. P., Cummings, J. A., Kara, A. B., Metzger, E. J., Shriver, J. F., et al. (2008). Eddy-resolving global ocean prediction. *Ocean Modeling in an Eddying Regime, Geophysical Monograph*, *177*, 353–381. https://doi.org/10.1029/177gm21

Janeković, I., Mihanović, H., Vilibić, I., & Tudor, M. (2014). Extreme cooling and dense water formation estimates in open and coastal regions of the Adriatic Sea during the winter of 2012. *Journal of Geophysical Research: Oceans*, *119*(5), 3200–3218. https://doi.org/10.1002/2014jc009865

Kara, A. B., Wallcraft, A. J., & Hurlburt, H. E. (2007). A correction for land contamination of atmospheric variables near land–sea boundaries. *Journal of Physical Oceanography*, *37*(4), 803–818. https://doi.org/10.1175/jpo2984.1

Katavouta, A., & Thompson, K. R. (2016). Downscaling ocean conditions with application to the Gulf of Maine, Scotian shelf and adjacent Deep Ocean. *Ocean Modelling*, *104*, 54–72. https://doi.org/10.1016/j.ocemod.2016.05.007

Killworth, P. D. (1996). Time interpolation of forcing fields in ocean models. *Journal of Physical Oceanography*, *26*(1), 136–143. https://doi.org/10.1175/1520-0485(1996)026<0136:tioffi>2.0.co;2

Ličer, M., Smerkol, P., Fettich, A., Ravdas, M., Papapostolou, A., Mantziafou, A., et al. (2016). Modeling the ocean and atmosphere during an extreme bora event in northern Adriatic using one-way and two-way atmosphere–ocean coupling. *Ocean Science*, *12*(1), 71–86. https://doi.org/10.5194/os-12-71-2016

Liu, F., Mikolajewicz, U., & Six, K. D. (2022). Drivers of the decadal variability of the north Ionian gyre upper layer circulation during 1910–2010: A regional modelling study. *Climate Dynamics*, *58*(7–8), 2065–2077. https://doi.org/10.1007/s00382-021-05714-y

Liu, Y., Donat, M. G., Rust, H. W., Alexander, L. V., & England, M. H. (2019). Decadal predictability of temperature and precipitation means and extremes in a perfect-model experiment. *Climate Dynamics*, *53*(7–8), 3711–3729. https://doi.org/10.1007/s00382-019-04734-z

Madec, G., Bourdallé-Badie, R., Bouttier, P.-A., Bricaud, C., Bruciaferri, D., Calvert, D., et al. (2017). Nemo ocean Engine.

Marchesiello, P., McWilliams, J. C., & Shchepetkin, A. (2001). Open boundary conditions for long-term integration of regional Oceanic models. *Ocean Modelling*, *3*(1–2), 1–20. https://doi.org/10.1016/s1463-5003(00)00013-5

Masina, S., & Pinardi, N. (1994). Mesoscale data assimilation studies in the middle Adriatic Sea. *Continental Shelf Research*, *14*(12), 1293–1310. https://doi.org/10.1016/0278-4343(94)90049-3

Mihanović, H., Vilibić, I., Carniel, S., Tudor, M., Russo, A., Bergamasco, A., et al. (2013). Exceptional dense water formation on the Adriatic shelf in the winter of 2012. *Ocean Science*, *9*(3), 561–572. https://doi.org/10.5194/os-9-561-2013

Oddo, P., & Guarnieri, A. (2011). A study of the hydrographic conditions in the Adriatic Sea from numerical modelling and direct observations (2000–2008). *Ocean Science*, *7*(5), 549–567. https://doi.org/10.5194/os-7-549-2011

Oddo, P., Pinardi, N., & Zavatarelli, M. (2005). A numerical study of the interannual variability of the Adriatic Sea (2000–2002). *Science of the Total Environment*, *353*(1–3), 39–56. https://doi.org/10.1016/j.scitotenv.2005.09.061

Oppenheim, A. V. (1999). *Discrete-time signal processing*. Pearson Education India.

Ortega, P., Guilyardi, E., Swingedouw, D., Mignot, J., & Nguyen, S. (2017). Reconstructing extreme AMOC events through nudging of the ocean surface: A perfect model approach. *Climate Dynamics*, *49*(9), 3425–3441. https://doi.org/10.1007/s00382-017-3521-4

Paklar, G. B., Isakov, V., Koračin, D., Kourafalou, V., & Orlić, M. (2001). A case study of bora-driven flow and density changes on the Adriatic shelf (January 1987). *Continental Shelf Research*, *21*(16–17), 1751–1783. https://doi.org/10.1016/s0278-4343(01)00029-2

Paschini, E., Artegiani, A., & Pinardi, N. (1993). The mesoscale eddy field of the middle Adriatic Sea during fall 1988. *Deep Sea Research Part I: Oceanographic Research Papers*, *40*(7), 1365–1377. https://doi.org/10.1016/0967-0637(93)90117-1

Persechino, A., Mignot, J., Swingedouw, D., Labetoulle, S., & Guilyardi, E. (2013). Decadal predictability of the Atlantic meridional overturning circulation and climate in the IPSL-CM5A-LR model. *Climate Dynamics*, *40*(9), 2359–2380. https://doi.org/10.1007/s00382-012-1466-1

Pham, V. S., & Hwang, J. H. (2020). Effects and recovery of small-scale fluctuations in one-way nesting for regional ocean modeling. *Ocean Modelling*, *145*, 101524. https://doi.org/10.1016/j.ocemod.2019.101524

Pham, V. S., Hwang, J. H., & Ku, H. (2016). Optimizing dynamic downscaling in one-way nesting using a regional ocean model. *Ocean Modelling*, *106*, 104–120. https://doi.org/10.1016/j.ocemod.2016.09.009

Pinardi, N., Allen, I., Demirov, E., De Mey, P., Korres, G., Lascaratos, A., et al. (2003). The Mediterranean ocean forecasting system: First phase of implementation (1998–2001). *Annales Geophysicae*, *21*(1), 3–20. https://doi.org/10.5194/angeo-21-3-2003

Pinardi, N., Arneri, E., Crise, A., Ravaioli, M., & Zavatarelli, M. (2006). The physical, sedimentary and ecological structure and variability of shelf areas in the Mediterranean Sea (27). *Sea*, *14*, 1243–1330.

Pinardi, N., & Masetti, E. (2000). Variability of the large scale general circulation of the Mediterranean Sea from observations and modelling: A review. *Palaeogeography, Palaeoclimatology, Palaeoecology*, *158*(3–4), 153–173. https://doi.org/10.1016/s0031-0182(00)00048-1

Pinardi, N., Zavatarelli, M., Adani, M., Coppini, G., Fratianni, C., Oddo, P., et al. (2015). Mediterranean Sea large-scale low-frequency ocean variability and water mass formation rates from 1987 to 2007: A retrospective analysis. *Progress in Oceanography*, *132*, 318–332. https://doi.org/10.1016/j.pocean.2013.11.003

Poulain, P.-M. (2001). Adriatic Sea surface circulation as derived from drifter data between 1990 and 1999. *Journal of Marine Systems*, *29*(1–4), 3–32. https://doi.org/10.1016/s0924-7963(01)00007-0

Pranić, P., Denamiel, C., Janeković, I., & Vilibić, I. (2023). Multi-model analysis of the Adriatic dense-water dynamics. *Ocean Science*, *19*(3), 649–670. https://doi.org/10.5194/os-19-649-2023

Pranić, P., Denamiel, C., & Vilibić, I. (2021). Performance of the Adriatic Sea and Coast (Adrisc) climate component–a COAWST v3. 3-Based coupled atmosphere-ocean modelling suite: Ocean part. *Geoscientific Model Development Discussions, 2021*, 1–46.

Pranić, P., Denamiel, C., & Vilibić, I. (2024). Kilometer-scale assessment of the Adriatic dense water multi-decadal dynamics. *Journal of Geophysical Research: Oceans*, *129*(10), e2024JC021182. https://doi.org/10.1029/2024jc021182

Provini, A., Crosa, G., & Marchetti, R. (1992). Nutrient export from the Po and Adige River basins over the last 20 years. In *Marine coastal eutrophication* (pp. 291–313). Elsevier.

Shchepetkin, A. F., & McWilliams, J. C. (2005). The Regional Oceanic Modeling System (ROMS): A split-explicit, free-surface, topography-following-coordinate oceanic model. *Ocean Modelling*, *9*(4), 347–404. https://doi.org/10.1016/j.ocemod.2004.08.002

Simoncelli, S., Pinardi, N., Oddo, P., Mariano, A. J., Montanari, G., Rinaldi, A., & Deserti, M. (2011). Coastal rapid environmental assessment in the northern Adriatic Sea. *Dynamics of Atmospheres and Oceans*, *52*(1–2), 250–283. https://doi.org/10.1016/j.dynatmoce.2011.04.004

Skamarock, W. C., Duda, M. G., Ha, S., & Park, S.-H. (2018). Limited-area atmospheric modeling using an unstructured mesh. *Monthly Weather Review*, *146*(10), 3445–3460. https://doi.org/10.1175/mwr-d-18-0155.1

Torresan, S., Gallina, V., Gualdi, S., Bellafiore, D., Umgiesser, G., Carniel, S., et al. (2019). Assessment of climate change impacts in the North Adriatic coastal area. Part I: A multi-model chain for the definition of climate change hazard scenarios. *Water*, *11*(6), 1157. https://doi.org/10.3390/w11061157

Umgiesser, G., Bajo, M., Ferrarin, C., Cucco, A., Lionello, P., Zanchettin, D., et al. (2021). The prediction of floods in Venice: Methods, models and uncertainty. *Natural Hazards and Earth System Sciences*, *21*(8), 2679–2704. https://doi.org/10.5194/nhess-21-2679-2021

Umgiesser, G., Ferrarin, C., Bajo, M., Bellafiore, D., Cucco, A., De Pascalis, F., et al. (2022). Hydrodynamic modelling in marginal and coastal seas—the case of the Adriatic Sea as a permanent laboratory for numerical approach. *Ocean Modelling*, *179*, 102123. https://doi.org/10.1016/j.ocemod.2022.102123

Verri, G., Furnari, L., Gunduz, M., Senatore, A., Santos da Costa, V., De Lorenzis, A., et al. (2024). Climate projections of the Adriatic Sea: Role of river release. *Frontiers in Climate*, *6*, 1368413. https://doi.org/10.3389/fclim.2024.1368413

Verri, G., Pinardi, N., Bryan, F., Tseng, Y.-h., Coppini, G., & Clementi, E. (2020). A box model to represent estuarine dynamics in mesoscale resolution ocean models. *Ocean Modelling*, *148*, 101587. https://doi.org/10.1016/j.ocemod.2020.101587

Verri, G., Pinardi, N., Oddo, P., Ciliberti, S. A., & Coppini, G. (2018). River runoff influences on the central Mediterranean overturning circulation. *Climate Dynamics*, *50*(5–6), 1675–1703. https://doi.org/10.1007/s00382-017-3715-9

Vested, H. J., Berg, P., & Uhrenholdt, T. (1998). Dense water formation in the northern Adriatic. *Journal of Marine Systems*, *18*(1–3), 135–160. https://doi.org/10.1016/s0924-7963(98)00009-8

Vilibić, I., Mihanović, H., Janeković, I., & Šepić, J. (2016). Modelling the formation of dense water in the northern Adriatic: Sensitivity studies. *Ocean Modelling*, *101*, 17–29. https://doi.org/10.1016/j.ocemod.2016.03.001

Vilibić, I., & Orlić, M. (2002). Adriatic water masses, their rates of formation and transport through the Otranto strait. *Deep Sea Research Part I: Oceanographic Research Papers*, *49*(8), 1321–1340. https://doi.org/10.1016/s0967-0637(02)00028-6

Vilibić, I., & Supić, N. (2005). Dense water generation on a shelf: The case of the Adriatic Sea. *Ocean Dynamics*, *55*(5–6), 403–415. https://doi.org/10.1007/s10236-005-0030-5

Vilibić, I., Zemunik, P., Dunić, N., & Mihanović, H. (2020). Local and remote drivers of the observed thermohaline variability on the Northern Adriatic shelf (Mediterranean Sea). *Continental Shelf Research*, *199*, 104110. https://doi.org/10.1016/j.csr.2020.104110

Yari, S., Kovačević, V., Cardin, V., Gačić, M., & Bryden, H. L. (2012). Direct estimate of water, heat, and salt transport through the Strait of Otranto. *Journal of Geophysical Research*, *117*(C9). https://doi.org/10.1029/2012jc007936

Zavatarelli, M., & Pinardi, N. (2003). The Adriatic Sea modelling system: A nested approach. In *Annales Geophysicae* (Vol. 21(1), pp. 345–364). https://doi.org/10.5194/angeo-21-345-2003

Zore-Armanda, M. (1963). Mixing of three water types in the South Adriatic. *Rapports et procès-verbaux des réunions de la Commission Internationale pour l'Exploration Scientifique de la Mer Méditerranée*, *17*, 879–885.